CRYSTAL GROWTH & DESIGN
2003
VOL. 3, NO. 4
615−619

Single-Crystal Growth of Magnesium Orthovanadate, $Mg_3(VO_4)_2$, by the Optical Floating Zone Technique

Jason D. Pless,[†] Natasha Erdman,[‡] Donggeun Ko,[†,§] Laurance D. Marks,[‡] Peter C. Stair,[†] and Kenneth R. Poeppelmeier*,[†]

Institute for Environmental Catalysis, Department of Chemistry, Northwestern University, 2145 Sheridan Road, Evanston, Illinois 60208-3113, Institute for Environmental Catalysis, Department of Materials Science and Engineering, Northwestern University, 2137 Sheridan Road, Evanston, Illinois 60208-3000, and Research and Development Center, Rubicon Technology Inc., Bannockburn, Illinois 60015

Received February 20, 2003

ABSTRACT: Magnesium orthovanadate crystals (< Φ 5 mm × L 55 mm) with a well-defined crystallographic orientation have been grown successfully in a four-mirror optical floating zone furnace. The crystals grow in the [010] direction. The transparent orange-brown crystals develop a predominant facet along the [20−1] during the crystal growth and cleave along the [20−1] and [100] directions.

Introduction

Mixed metal oxides exhibit a wide range of properties that make them useful materials for many modern industrial applications, including catalysis. Since they are ceramic materials, they commonly are used as polycrystalline or finely dispersed, high surface area nanocrystalline solids. Often, for purposes of research, experiments are conducted on polycrystalline samples when single crystals would be preferable. However, large single crystals are difficult to obtain because mixed metal oxides, in many cases, melt incongruently, exhibit crystallographic phase transitions, or contain a volatile component. Nonetheless, the effort required to prepare single-crystal samples is often warranted by the uniformity of composition and the precise orientation of a crystal.

Magnesium orthovanadate is of interest because of its catalytic properties[1−10] and unique structure.[11,12] An extraordinary characteristic of magnesium orthovanadate is its structural similarity with its reduced phase, $Mg_3V_2O_6$,[12] implying that the surface of the oxide can undergo multiple reduction and oxidation cycles. Upon reduction in hydrogen, the cation-deficient spinel, $Mg_3V_2O_8$, transforms to a cation-stuffed spinel, $Mg_3V_2O_6$. Specifically, the vanadium atoms migrate from tetrahedral sites to octahedral interstices, while the octahedral magnesium atoms rearrange to equally occupy the tetrahedral and octahedral sites.[12] Similar topochemical behavior has been exhibited by thin films of $Mg_3(VO_4)_2$ when reduction occurs with propane,[13] confirming that this system is an excellent model catalyst.

Although magnesium orthovanadate has been shown to convert light alkanes to their respective alkenes, little is known about the active sites and the chemistry that occurs on the oxide's surface. Reactivity can be influenced by the inter-related parameters of composition, crystal orientation, and surface structure, making it difficult to examine and discern the effect of any one on the catalytic activity. Knowledge of the active surface(s)' atomic structure and of the adsorbed reactants, intermediates, and products is necessary for a molecular understanding of catalytic oxidative dehydrogenation. Single-crystal samples with well-defined crystallographic orientations can help to understand these materials with the goal of improving their selectivity. The atomic structure can be determined with high-resolution electron microscopy (HREM), while the identification of reactants, intermediates, and products can be studied with surface science techniques. A single crystal, free of structural defects, or with a known amount of well-defined defects, reduces the surface complexity and would enable fundamental studies of the surface and its active sites. Recently, the surface atomic structure of $SrTiO_3$ has been solved using a combination of single-crystal HREM and direct methods.[14]

Large magnesium orthovanadate single crystals are challenging to grow because $Mg_3(VO_4)_2$ melts incongruently. Traditionally, single crystals have been grown using the flux method.[12] However, this method results in crystals imbedded in the flux, which are too small (<2 mm)[12] for the required surface characterizations. In contrast to the flux method, the optical floating zone method, in the traveling solvent zone configuration, can be used to grow large single crystals of incongruently melting phases. The compositional change that occurs in incongruently melting systems is compensated by the steady state that is established between the liquid and the boundary where crystallization ensues. Additional advantages provided by the optical floating zone method include no contamination as a result of a crucible free operation and a steep temperature gradient along the vertical direction, which allows for faster and more stable crystal growth.

Experimental Procedures

Crystal Growth. Magnesium orthovanadate was prepared by calcining mixed, stoichiometric amounts of MgO (Alfa Aesar 99.95%) and V_2O_5 (Alfa Aesar 99.995%) at 900 °C. Support

* To whom correspondence should be addressed. Phone: (847) 491-3505. Fax: (847) 491-7713. E-mail: krp@northwestern.edu.
[†] Department of Chemistry, Northwestern University.
[‡] Department of Materials Science and Engineering, Northwestern University.
[§] Rubicon Technology Inc.

10.1021/cg0340289 CCC: $25.00
Published on Web 05/15/2003

and feed rods for the crystal growth were formed by hydrostatically pressing (70 kPa) the $Mg_3(VO_4)_2$ into a rubber tube of cylindrical shape (6 mm in diameter, 60−90 mm long). The rods were sintered in air at 1125 °C (24 h) to form dense, polycrystalline rods. Crystal growth experiments were carried out using an optical image furnace (CSI FZ-T-10000-H-VI-VP, Crystal Systems, Inc., Japan) that was equipped with four 300 W tungsten halide lamps and four elliptical mirrors.

Crystal Characterization. Phase identification was made using powder X-ray diffraction. The data were collected (0.05°/1 s for $10° < 2\theta < 70°$) at room temperature on a Rigaku X-ray diffractometer using a Cu Kα radiation and a nickel filter. A single crystal was mounted on a glass fiber for study by single-crystal X-ray diffraction. All measurements were made on a Bruker Smart 1000 with a CCD detection plate and a graphite monochromator at a temperature of −120 °C. The structure was refined using the TEXSAN software package.[15] Differential thermal analysis (DTA) was performed on a TA Instruments DSC 2910 differential scanning calorimeter. The DTA heating profile consisted of two cycles where the crystal was heated from room temperature to 1100 °C at 10 °C/min and cooled to 25 °C at 10 °C/min. The orientations of naturally occurring facets and the growth direction were determined using Laue backscattering diffraction. The orientation of the crystal facets was determined using the Orient Express software package.[16] The crystals were mounted 30 mm from the detector, and a molybdenum source was operated at 19 kV and 21 mA. Electron backscattering diffraction (EBSD) was also implemented to determine the crystallographic orientation of naturally occurring facets. The samples were polished, ultrasonically cleaned, and then coated with ∼50 Å of carbon to prevent charging effects in the SEM. The EBSD patterns were collected at 20 kV using a Hitachi S-570 SEM with LaB_6 source equipped with TexSEM Laboratories EBSD equipment.

Results and Discussion

Successful growth of a single crystal involves a stable liquid zone. Achieving a stable liquid zone requires dense, chemically homogeneous, straight, and precisely aligned feed and support rods. If the starting feed rod is not adequately dense, then more liquid can crystallize than will be replenished from the melting feed rod, or the liquid can penetrate into the feed rod by capillary action. In either situation, the diminishing volume of liquid will cause the feed rod to disconnect eventually from the support rod. Crooked or imprecisely aligned rods rotate out of the center axis during crystal growth and disturb the stability of the liquid zone.

Uniformly dense, chemically homogeneous straight feed and support rods were prepared by the process described above. The rods were aligned in the furnace by attaching the feed rod to the upper shaft of the furnace and rigidly fixing the support rod onto the lower shaft of the furnace. This method of rod preparation enables a stable liquid zone to form and a successful crystal growth to occur.

Crystal growth begins by melting the bottom of the feed rod and the top of the support rod, forming a liquid zone between the counter-rotating feed and support rods. Magnesium orthovanadate melts peritectically at 1159 °C, decomposing into crystalline magnesium oxide and a liquid of peritectic liquidus composition.[17] Volatilization of the liquid is eliminated by reducing the power of the halogen lamps to a limit permitting an undisturbed rotation. The crystal growth starts with MgO crystallization on top of the support rod and proceeds with the upward translation of the mirror stage. The liquid composition continuously changes until a steady state is established between the liquid and the crystallized magnesium oxide. At this point, a dynamic steady state is established, and crystallization of $Mg_3(VO_4)_2$ commences. The crystallized $Mg_3(VO_4)_2$ is replenished simultaneously from the feed rod. The crystal growth is performed slowly to maintain equilibrium conditions, and by that, the continuous growth of crystalline magnesium orthovanadate from a liquid of a different composition results.

Transparent orange-brown crystals (Figure 1) were grown on polycrystalline supports of $Mg_3(VO_4)_2$ or on single crystals oriented with the [20−1] perpendicular to the growth direction. When growth begins, multiple

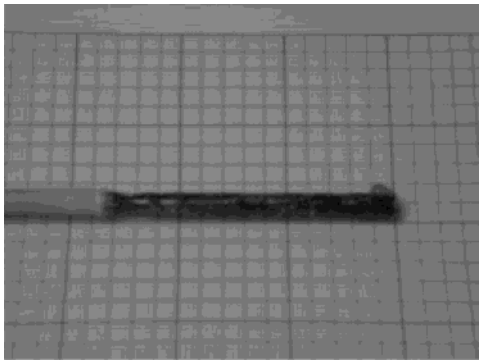

Figure 1. Magneisum orthovanadate crystal grown in the floating zone furnace. Each partition represents 5 mm.

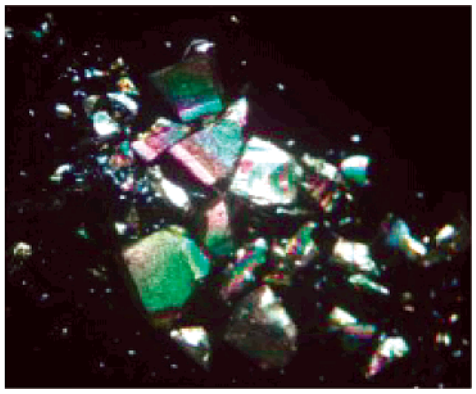

Figure 2. Twinned crystals under polarized light.

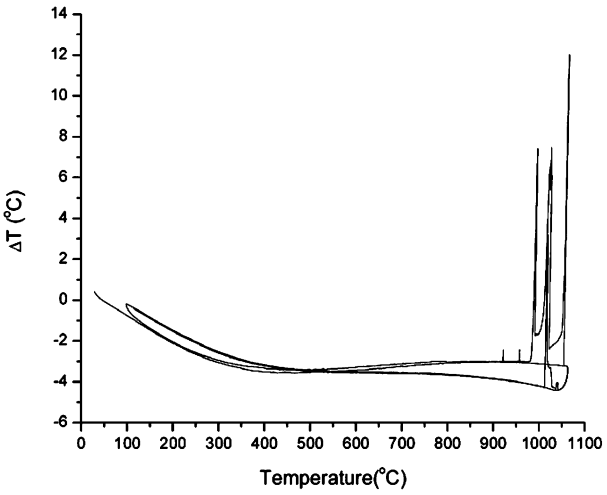

Figure 3. DTA of thermally activated, irreversible, kinetic process (detwinning).

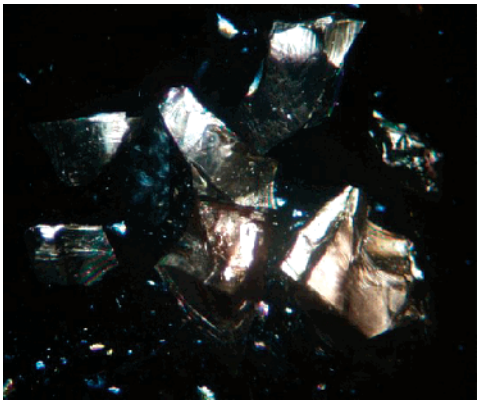

Figure 4. Single crystals under polarized light.

nucleation sites were observed to form. The growth rate and speed of the counter-rotating support and feed rods were varied to minimize the number of crystal domains. The typical growth rate adopted was 0.5 mm/h. Faster rates result in several smaller crystalline domains, while slower rates did not reduce the number of crystal domains. Further optimization was achieved when both the support and the feed rods were counter-rotated between 16.0 and 18.0 rpm. At these speeds and growth rate, the number of nucleation sites was minimized, and the largest diameter crystals were obtained. Additionally, the crystal diameter was reduced with a necking technique, and the number of crystal domains decreased. With these optimizations, the crystal rod was composed of several large domains. The largest crystal fragments were ~Φ 5 mm × L 55 mm. In addition, the growth atmosphere was varied from a flow of 25% O_2/75% N_2 to 100% O_2. Crystals grown in 25% O_2 are darker in color than crystals grown in oxygen. Presumably, the oxygen atmosphere stabilizes the vanadium with respect to trace reduction.

Crystal twin planes were revealed with an optical microscope. The crystals appeared multicolored under polarized light (Figure 2). The possibility that the crystals are twinned was examined with DTA (Figure 3). Exothermic peaks occurred above 900 °C during the first cycle and did not appear during the second cycle, evidence of a thermally activated, irreversible process. In contrast, a reversible thermodynamic process would exhibit both an endothermic and an exothermic peak on heating and cooling, respectively, near the transition temperature. The observed exothermic transitions were attributed to a detwinning process (i.e., the removal of twin planes). The treated crystals were reexamined under polarized light and found to extinguish light uniformly, which indicates that the twin boundaries have been removed (Figure 4). This information was used to remove twinning in other crystals by heating them at 1000 °C under flowing O_2.

Powder X-ray diffraction was performed to determine the purity of the crystal samples. The powder diffraction patterns for crushed crystals grown in both 25 and 100% O_2 show no evidence of contamination from another phase (Figure 5). The peak positions of the diffraction patterns match the calculated pattern taken from Krishnamachari and Calvo.[11] Single crystal X-ray data (Table 1), for the crystal grown in pure oxygen, was refined and agrees with the previously published structure.[11] The final R and R_w values are 0.030 and 0.035, respectively. The atomic positions with corresponding temperature factors are shown in Table 2.

The crystals develop a predominant facet (Figure 6) during the growth. Laue diffraction was employed to determine the orientations of the predominant facet and the growth direction. The obtained pattern for the predominant facet (Figure 7) was indexed to [20−1] direction, and the growth direction (Figure 8) was indexed to [010]. The cleavage planes were indexed to

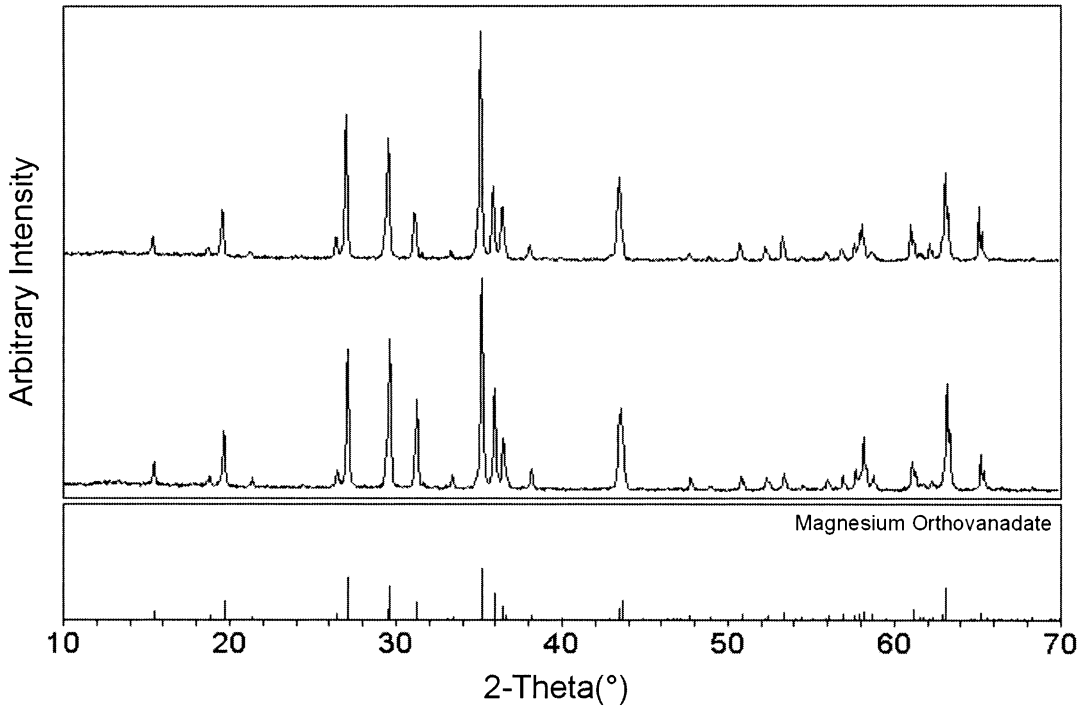

Figure 5. PXRD spectra of crystals grown in O_2 (top) and 75% N_2/25% O_2 (middle) as compared to the calculated pattern (bottom).

Table 1. Summary of Crystallographic Data

chemical formula	$Mg_3(VO_4)_2$
formula weight	302.79
space group, Z	$Cmca$ (64), 4
a	6.0495(8) Å
b	11.426(2) Å
c	8.303(1) Å
D_{calc}, D_{meas}[b] (g/cm^3)	3.504, 3.48
μ(Mo Kα)	35.91 cm^{-1}
$2\theta_{max}$	56.6°
no. reflections meas.	total: 2662
	unique: 432
$I > 3.00\sigma(I)$	313
R (R_w)[a]	0.030 (0.035)
goodness of fit	2.32

[a] $R = \sum||F_{obs}| - |F_{calc}||/\sum|F_{obs}|$; $R_w = [\sum w(|F_{obs}| - |F_{calc}|)^2/\sum|F_{obs}|^2]^{0.5}$. [b] Measured at room temperature.

Table 2. Atomic Positions for $Mg_3(VO_4)_2$

atom	Wyckoff position	x	y	z	B_{eq}[a]
V(1)	8f	0	0.3797(8)	0.1209(8)	0.42(1)
Mg(1)	4b	0	0	0	0.55(3)
Mg(2)	8e	0.25	0.1353(1)	0.25	0.52(2)
O(1)	8f	0	0.2514(2)	0.2274(3)	0.54(5)
O(2)	8f	0	0.0037(2)	0.2442(3)	0.51(5)
O(3)	16g	0.2723(3)	0.1179(1)	0.9974(2)	0.53(3)

[a] $B_{eq} = 8/3\pi^2(U_{11}(aa^*)^2 + U_{22}(bb^*)^2 + U_{33}(cc^*)^2 + U_{12}aa^*bb^*\cos\gamma + U_{13}aa^*cc^*\cos\beta + U_{23}bb^*cc^*\cos\alpha)$.

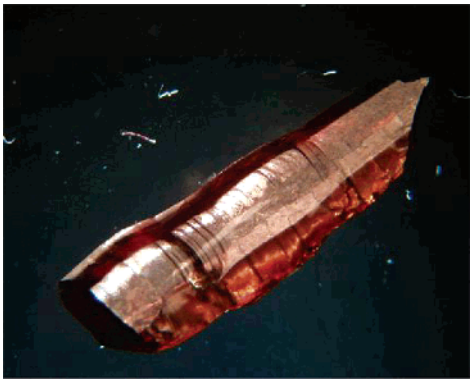

Figure 6. Predominant facet that forms during the crystal growth.

the [20−1] and [100] directions on an X-ray diffractometer. Figures showing the unit cell oriented in the three directions can be seen in the Supporting Information. The crystals can be oriented and cut to obtain other low index surfaces, enabling the fundamental study of the active sites for a better understanding of the surface reactivity.

Electron backscattering diffraction (EBSD) was also implemented to verify the crystallographic orientation of the naturally occurring facets on the $Mg_3(VO_4)_2$ single crystals. The sample preparation for EBSD is crucial since the diffraction information originates in approximately a 20 nm layer at the surface, corresponding to the penetration depth for backscattered electrons. The naturally forming facets were identified, and the crystal surfaces were polished to investigate those facets. For this experiment, the electron beam is stationary and incident to the surface of the sample at a glancing angle of less than 35°; the geometry is maintained to ensure a high backscattered signal coefficient. The resulting pattern is collected on a phosphor screen. First, a background signal from a larger area was collected, and then the beam was focused on a specific site and an

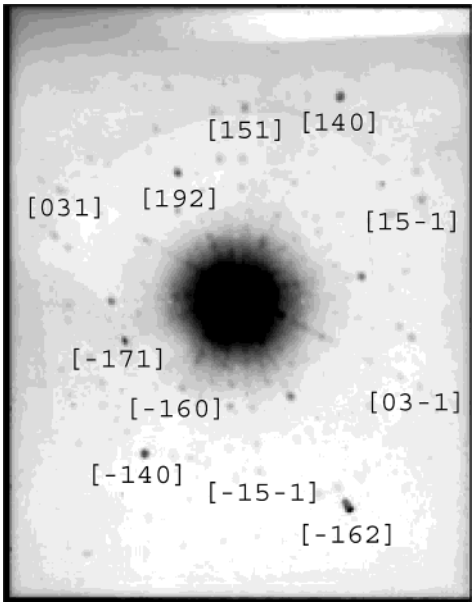

Figure 7. Laue back-reflection of the predominant facet that develops during the growth. The direction of the facet is indexed to [20−1].

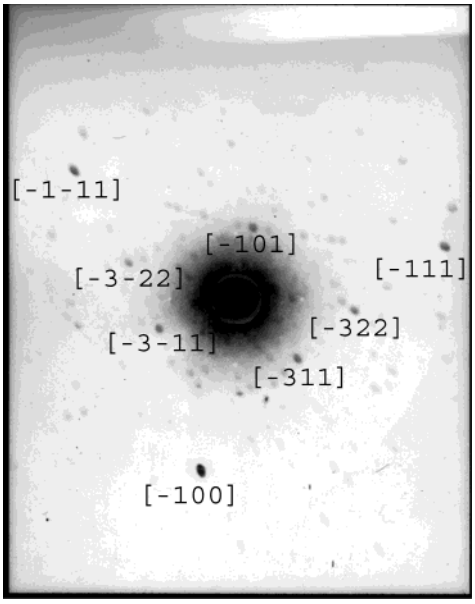

Figure 8. Laue back-reflection of the crystal growth direction indexed to the [010] direction.

EBSD pattern was obtained. The resulting Kikuchi map was analyzed according to the known space group and crystal system of the material to calculate the crystal orientation through measurement of the angles between the different Kikuchi lines. The resulting EBSD pattern is shown in Figure 9. The obtained pattern corresponds to [20−1] zone axis, agreeing with the results from Laue diffraction.

Conclusion

The growth of large single crystals of magnesium orthovanadate consists of finding the correct set of conditions for a stable liquid region. The growth conditions for high quality $Mg_3(VO_4)_2$ single crystals have been presented. X-ray characterization shows agree-

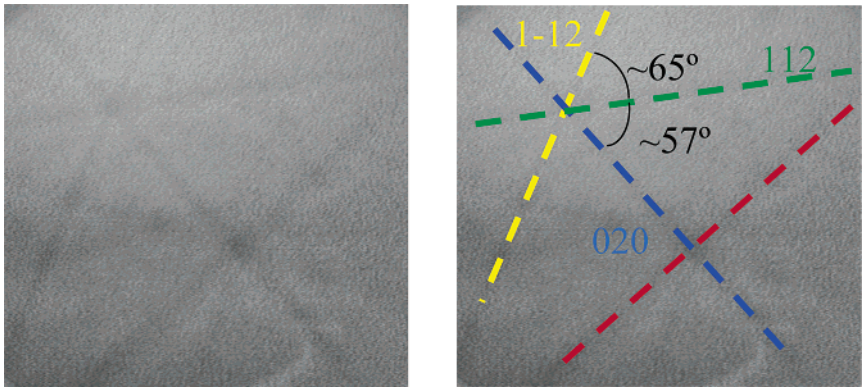

Figure 9. Electron backscattering diffraction of the [20−1] direction. (A) The original EBSD pattern with inverted contrast. (B) Kikuchi lines are drawn in and indexed.

ment with the structure published by Krishnamachari and Calvo.[11] There is no evidence of contamination by another phase, but the crystal is composed of several domains. The single crystals grow in the [010] direction and develop a facet in the [20−1] direction during the crystal growth.

The results of this study will make it possible to grow large single crystals of other related vanadates. For example, pure polycrystalline samples of $Mn_3(VO_4)_2$ and $AlVO_4$ have been reported as challenging to prepare.[18,19] As in the case of $Mn_3(VO_4)_2$, the oxygen partial pressure is a critical factor affecting the crystal growth. From the results of Wang et al.,[18] a crystal of $Mn_3(VO_4)_2$ should be grown in an Ar atmosphere. Aluminum orthovanadate, $AlVO_4$, exhibits a peritectic reaction at 765 °C.[20] Thus, it may be possible to grow a crystal of $AlVO_4$ in a flux that melts below 765 °C. In general, phases with an increasing number of elements are inherently more difficult to grow.[21−24] Understanding the factors that affect crystal synthesis will enable the growth of large single crystals of materials that are currently difficult to grow.

Acknowledgment. The authors thank Charlotte L. Stern for assistance with crystallographic measurements. The authors gratefully acknowledge support by the EMSI program of the National Science Foundation and the U.S. Department of Energy Office of Science at the Northwestern University Institute for Environmental Catalysis and made use of the Central Facilities supported by the MRSEC program of the National Science Foundation (Grant DMR-0076097) at the Materials Research Center of Northwestern University.

Supporting Information Available: Photographs of the optical floating zone furnace, X-ray crystallographic information file (CIF), and atomic drawings for the predominate facet, growth direction, and cleavage planes. This material is available free of charge via the Internet at http://pubs.acs.org.

References

(1) Chaar, M. A.; Patel, D.; Kung, M. C.; Kung, H. H. *J. Catal.* **1987**, *105*, 483−498.
(2) Chaar, M. A.; Patel, D.; Kung, H. H. *J. Catal.* **1988**, *109*, 463−467.
(3) Nguyen, K. T.; Kung, H. H. *J. Catal.* **1990**, *122*, 415−428.
(4) Sam, D. S. H.; Soenen, V.; Volta, J. C. *J. Catal.* **1990**, *123*, 417−435.
(5) Guerrero-Ruiz, A.; Rodriguez-Ramos, I.; Fierro, J. L. G.; Soenen, V.; Herrmann, J. M.; Volta, J. C. *Stud. Surf. Sci. Catal.* **1992**, *72*, 203-212.
(6) Corma, A.; Lopez Nieto, J. M.; Paredes, N. *J. Catal.* **1993**, *144*, 425−438.
(7) Gao, X.; Ruiz, P.; Xin, Q.; Guo, X.; Delmon, B. *J. Catal.* **1994**, *148*, 56−67.
(8) Fang, Z.; Weng, W.; Wan, H.; Tsai, K. *Fenzi Cuihua* **1995**, *9*, 401−410.
(9) Carrazan, S. R. G.; Peres, C.; Bernard, J. P.; Ruwet, M.; Ruiz, P.; Delmon, B. *J. Catal.* **1996**, *158*, 452−476.
(10) Lemonidou, A. A.; Tjatjopoulos, G. J.; Vasalos, I. A. *Catal. Today* **1998**, *45*, 65−71.
(11) Krishnamachari, N.; Calvo, C. *Can. J. Chem.* **1971**, *49*, 1629−1637.
(12) Wang, X.; Zhang, H.; Sinkler, W.; Poeppelmeier, K. R.; Marks, L. D. *J. Alloys Compd.* **1998**, *270*, 88−94.
(13) Ruffner, J. A.; Sault, A. G.; Rodriguez, M. A.; Tissot, R. G., Jr. *J. Vac. Sci. Technol. A* **2000**, *18*, 1928−1932.
(14) Erdman, N.; Poeppelmeier, K. R.; Asta, M.; Warschkow, O.; Ellis, D. E.; Marks, L. D. *Nature (London)* **2002**, *419*, 55−58.
(15) *TEXSAN-TEXRAY* Molecular Structure Corp., 1985.
(16) Bochu, J. L. a. B. *Laboratories des Materiaux et du Genie Physique de l'Ecole Superieure de Physique de Grenoble*, http://www.inpg.fr/LMPG/ 2001.
(17) Wollast, R.; Tazairt, A. *Silicates Ind.* **1969**, *34*, 37−45.
(18) Wang, X.; Liu, Z.; Ambrosini, A.; Maignan, A.; Stern, C. L.; Poeppelmeier, K. R.; Dravid, V. P. *Solid State Sci.* **2000**, *2*, 99−107.
(19) Nielson, U. G.; Boisen, A.; Brorson, M.; Jacobsen, C. J. H.; Jakobsen, H. J.; Skibsted, J. *Inorg. Chem.* **2002**, *41*, 6432−6439.
(20) Touboul, M.; Popot, A. *J. Therm. Anal.* **1986**, *31*, 117−124.
(21) Wang, X.; Heier, K. R.; Stern, C. L.; Poeppelmeier, K. R. *J. Alloys Compd.* **1998**, *267*, 79−85.
(22) Wang, X.; Vander Griend, D. A.; Stern, C. L.; Poeppelmeier, K. R. *J. Alloys Compd.* **2000**, *298*, 119−124.
(23) Wang, X.; Vander Griend, D. A.; Stern, C. L.; Poeppelmeier, K. R. *Inorg. Chem.* **2000**, *39*, 136−140.
(24) Wang, X.; Norquist, A. J.; Pless, J.; Stern, C. L.; Vander Griend, D. A.; Poeppelmeier, K. R. *J. Alloys Compd.* **2002**, *338*, 26−31.

CG0340289